

1 **Response to reviewers of Jenner et al., Plasma density gradients at the**
2 **edge of polar ionospheric holes: The absence of phase scintillation**

3 We thank both reviewers for their detailed and careful review of this paper. We note that both
4 reviewers stated that this paper is clear, well written and worthy of publication after minor
5 revisions. We thank both reviewers for this comment.

6 The reviewers have raised a number of important points. All of these have been addressed
7 below, and a revised version of the manuscript has been submitted. For the convenience of
8 the reviewers, two versions have been uploaded. 'Jenner_et_al_track_changes' shows every
9 individual change and 'Jenner_et_al_revised' has all changes implemented, with major
10 changes highlighted in yellow. We believe that these revisions substantially enhance the
11 manuscript.

12 **Detailed response to comments from Anonymous Reviewer 1**

13 **Comment 1: The meaning and definition of phase scintillation at high-latitudes**

14 The reviewer commented that this was missing from the introduction. We had omitted this in the
15 interests of concision, but the review is absolutely correct that it needs to be included. A brief but
16 comprehensive summary is now given in lines 114-128 using many of the references suggested by the
17 reviewer.

18 **Comment 2: Title of the paper**

19 We agree that the suggested modification gives a better title for this paper, and have amended the
20 title.

21 **Comment 3: Would phase scintillation be observed at lower time windows?**

22 This is an excellent suggestion, and one worthy of investigation. The effect of the length of the sampling
23 window on phase scintillation indices would be a fascinating next step, and one which shall certainly
24 be investigated in future experiments. A comment to this effect has been added in lines 422-429. As
25 only the scintillation indices (and not the raw 50 Hz data) have been archived it is not possible to
26 investigate within this study, and we have used the 60 second window which is commonly used within
27 the community.

28 **Comment 4: Abstract should refer to GNSS receivers, rather than GNSS satellites**

29 Agreed. This change has been made (line 19). Similar changes have been made to lines 261 and 438.

30 **Comment 5: Figure 5 is cited before figures 2, 3 and 4.**

31 Thank you for pointing this out. Line 181 has been re-phrased accordingly.

32 **Comment 6: ACE data is available time-shifted to the bow shock**

33 Indeed it is. We have re-produced figures 1 & 6 and modified the associated text (lines 175-182 and
34 lines 284-288) accordingly.

35 **Comment 7: EISCAT data (figures 3, 8 and 10): Choice of colour scale and scaling of velocity data**

36 The reviewer suggested changing the colour scale on these plots from red-green-blue to red-white-
37 blue. We have retained the red-green-blue colour scale, as this is commonly used for EISCAT data and
38 so enables an easy comparison to other data sets in the published literature.

39 The reviewer also commented that, for Fig. 3 (bottom panel) “The adopted color code is not suitable
40 to catch positive/negative variations.” This is true, but the choice was deliberate. The same scale was
41 used for the velocity information in figures 3, 8 and 10. This was so that the difference between the
42 larger velocities in Fig. 10 for the radar observing at low elevation and the smaller (negligible) velocities
43 at high elevation (figures 3 and 8) could be clearly seen. However, we did not make this clear in the
44 paper, and thank the reviewer for their comment. We have amended the text in lines 203-208 and 321-
45 325 accordingly.

46 **Comment 8: Citation of chosen threshold for SigmaPhi**

47 A discussion of different thresholds (along with suitable citations) has been added to lines 276-280.

48 **Detailed response to comments from Anonymous Reviewer 2**

49 **Comment 1: Purpose of the paper as discussed in the abstract and conclusion**

50 The reviewer commented that “The conclusions are currently described in a rather vague way. In the
51 abstract, the last sentence “It may be that ...” should be revised. In the conclusions section, also the
52 last sentence should be revised.” We agree with this comment that the conclusions should be stronger,
53 and have revised lines 441-446 accordingly. We also amended lines 435-439 to enhance the clarity of
54 the paper. A corresponding change has been made in the abstract to line 23.

55 **Comment 2: Purpose of the paper as discussed in the introduction**

56 The reviewer commented that “It seems that the objective of the paper is to present observational
57 proof for the comment in Aarons (1982) as described in Lines 251-253. I recommend to add this to the
58 last part of the introduction.” We agree with this comment that this should be more explicit, and have
59 revised lines 134-135 accordingly.

60 **Comment 3: Minor typos / change of tense in lines 166, 170, 176, 200 and 227**

61 We thank the reviewer for identifying these. They have all been corrected in the revised manuscript,
62 with the corrections occurring in lines 270, 282, 285, 347 and 383 respectively.

63 **Comment 4: Table 1 should use the same exponent in each cell to enable easier comparisons**

64 Agreed. This change has been made.

65

66

67

68

69 Plasma density gradients at the edge 70 of polar ionospheric holes: **The** 71 **absence of phase scintillation**

72 **Luke A. Jenner**, ^[1], **Alan G. Wood** ^[1], **Gareth D. Dorrian** ^[1], **Kjellmar Oksavik** ^[2, 3],
73 **Timothy K. Yeoman** ^[4], **Alexandra R. Fogg** ^[4], and **Anthea J. Coster** ^[5]

74 ^[1] School of Science & Technology, Nottingham Trent University, Nottingham, UK.

75 ^[2] Birkeland Centre for Space Science, Department of Physics and Technology, University of Bergen,
76 Bergen, Norway

77 ^[3] Arctic Geophysics, University Centre in Svalbard, Longyearbyen, Norway

78 ^[4] Department of Physics and Astronomy, University of Leicester, Leicester, UK.

79 ^[5] MIT Haystack Observatory, Massachusetts, USA.

80

81 **Abstract**

82 Polar holes were observed in the high-latitude ionosphere during a series of multi-instrument
83 case studies close to the northern hemisphere winter solstice in 2014 and 2015. These holes
84 were observed during geomagnetically quiet conditions and under a range of solar activities
85 using the European Incoherent Scatter Scientific Association (EISCAT) Svalbard Radar (ESR)
86 and measurements from Global Navigational Satellite System **(GNSS) receivers**. Steep
87 electron density gradients have been associated with phase scintillation in previous studies,
88 however, no enhanced scintillation was detected within the electron density gradients at
89 these boundaries. It is suggested that the lack of phase scintillation may be due to low plasma
90 density levels and a lack of intense particle precipitation. It **is concluded** that both significant
91 electron density gradients and that plasma density levels above a certain threshold are
92 required for scintillation to occur.

93 **Introduction**

94 The F-region ionosphere is a weakly ionised plasma in the Earth's atmosphere extending from
95 an altitude of ~150 to ~500 km, above which it merges with Earth's plasmasphere. Large-scale
96 plasma structures with a horizontal extent of tens to hundreds of km are routinely observed
97 in the F-region high-latitude ionosphere (Tsunoda, 1988). One type of structure commonly
98 observed are polar cap patches, also referred to as patches, which are enhancements of
99 plasma density with at least twice the background value and have a horizontal spatial extent
100 of 100 km or greater (Crowley, 1996). Buchau et al. (1983) observed such patches of enhanced
101 ionisation drifting antisunward with the background plasma flow in the central region of the
102 polar cap at Thule, Greenland (77.5° N, 69.2° W; 85.4° MLAT, 32.4° MLON). The patch densities
103 were larger than could be produced due to the observed flux of precipitating particles, and it
104 was concluded that the patches were not produced locally by precipitation. Weber et al.
105 (1984) suggested that the patches were produced on the dayside at auroral or subauroral
106 latitudes and then convected antisunward to higher, polar latitudes. A comparison of average
107 maps of the electron density and high-latitude convection pattern suggested that solar-
108 produced plasma was drawn into the polar cap as a continuous density enhancement known
109 as the Tongue-of-Ionisation (TOI) (Foster et al., 1984). Several mechanisms have been
110 proposed to break a TOI into a series of patches, including variations in the high-latitude
111 convection pattern moving flux tubes in and out of sunlight (Anderson et al., 1988), expansion
112 and contraction of the high-latitude convection pattern in response to transient bursts of
113 reconnection drawing in plasma from different latitudes (Cowley and Lockwood, 1992;
114 Lockwood and Carlson, 1992; Carlson et al., 2002, 2004, 2006), variations in the y-component
115 of the Interplanetary Magnetic Field (IMF) drawing in plasma from different magnetic local
116 times (MLT) (Sojka et al., 1993), variation of the z-component of the IMF altering whether
117 plasma could be drawn in to the polar cap (Valladares et al., 1998), erosion of plasma densities
118 due to enhanced recombination during a flow channel event (Rodger et al., 1994; Valladares
119 et al., 1994), and modification of the density of the photoionised plasma transported into the
120 polar cap by particle precipitation (Walker et al., 1999; Millward et al., 1999). Patches have
121 been observed travelling thousands of kilometres across the polar regions (Weber, 1986;
122 Oksavik et al., 2010; Nishimura et al., 2014), and are primarily associated with times when the
123 z-component of the IMF is negative (Buchau and Reinisch, 1991).

124 Blobs are also plasma density enhancements, however, unlike patches, they occur outside the
125 polar cap. They are further categorised into boundary blobs, subauroral blobs, and auroral
126 blobs (Rino, 1983; Jin et al., 2016). Boundary blobs are found near the equatorward auroral
127 boundary, neighbouring the ionospheric trough's poleward wall. Parkinson et al. (2002)
128 observed patches leaving the polar cap, slowing in the antisunward direction and then
129 beginning to move zonally. It was suggested that these patches would form boundary blobs,
130 and this was later confirmed by Pryse et al. (2006) who compared the plasma density in a
131 polar cap patch to that within a boundary blob which the patch subsequently formed.
132 Subauroral blobs have a similar appearance to boundary blobs, however, they are found in
133 the ionospheric trough. Auroral blobs are found within the auroral oval and seem to be
134 longitudinally restricted. The most likely mechanism for their creation is particle precipitation
135 (Jones et al., 1997).

136 Not all ionospheric structures are enhancements of the background plasma; polar ionospheric
137 holes are regions of low plasma density. Brinton et al. (1978) observed a depletion of this kind
138 under conditions of low solar activity ($F_{10.7}=71$ sfu) and low magnetic activity ($K_p = 2$). This
139 depletion was also associated with a minimum of electron temperatures, indicating the
140 absence of local particle precipitation. Polar holes are generally located between 21 and 06
141 MLT and 70° - 80° magnetic latitude and typically have steep plasma density gradients at their
142 boundaries. They are believed to be produced when plasma in the high-latitude convection
143 pattern circulates in perpetual darkness. Plasma loss by recombination in the absence of a
144 plasma source causes density levels to drop. This idea is supported by the conditions under
145 which polar holes have generally been observed, namely quiet geomagnetic activity (K_p 2 or
146 less) when the contribution to the plasma densities from particle precipitation will be low
147 (Brinton et al., 1978). The electron densities inside of the polar holes are seen to reach a
148 minimum in the range of 10^8 - 10^{11} electrons·m⁻³ (Obara and Oya, 1989, Benson and
149 Grebowsky, 2001) and, while there is variation between holes, inside of a singular polar hole
150 the density level is very consistent.

151 Smaller scale structures can arise at steep plasma density gradients due to instability
152 processes such as the gradient-drift instability (GDI) (Keskinen and Ossakow, 1983) and the
153 velocity shear driven instability (Kelvin-Helmholtz instability, KHI). Carlson et al. (2008)
154 proposed and that the real process involves both mechanisms acting on different time scales.

155 The smaller scale (tens of meters to tens of kilometers) plasma density structures that arise
156 cause variations in the refractive index of the ionosphere. As a GNSS signal passes through
157 this region, refraction and/or diffraction of the radio wave causes fluctuations in the phase
158 and amplitude of the signal. Ionospheric scintillation is the rapid fluctuation of the received
159 signal which can disrupt applications using GNSS, as thoroughly reviewed by Hapgood (2017).
160 Since the second world war, large numbers of studies have shown the effect of ionospheric
161 irregularities on radio signals, as reviewed by Aarons (1982). The morphology of these
162 irregularities has been extensively studied at high-latitudes (e.g. Kersley, 1972), together with
163 the effects upon the propagation of radio signals in this region (e.g. Kersley et al., 1995).

164 More recently studies have focussed on Global Navigation Satellite System (GNSS)
165 frequencies, where scintillation poses a substantial threat to the integrity, availability and
166 accuracy of GNSS positioning, leading to positioning errors and service outages due to signal
167 tracking problems at the GNSS receiver. A direct connection between gradients in the Total
168 Electron Content (TEC) at the edge of a plasma stream with both phase and amplitude
169 scintillation has been observed (Mitchell et al., 2005) and plasma structuring caused by
170 auroral precipitation has been linked to the loss of signal lock by a GNSS receiver (Elmas et al.,
171 2011; Smith et al., 2008; Oksavik et al., 2015). A statistical study has shown an agreement
172 between both phase and amplitude scintillation with the asymmetric distribution of polar cap
173 patches around magnetic midnight (Spogli et al., 2009) and that auroral emissions correlate
174 with GNSS signal phase scintillation (Kinrade et al., 2013; van der Meeren et al., 2015). Phase
175 and amplitude scintillation can be associated with the larger spatial structures associated with
176 polar cap patches (Alfonsi et al., 2011). The climatology of ionospheric scintillation at polar
177 latitudes in the northern hemisphere was determined over almost two solar cycles, and the
178 dependence upon solar cycle, geomagnetic activity and solar wind conditions was shown by
179 De Francheschi et al. (2019). Phase scintillation is usually the dominant process at high latitudes
180 (Spogli et al., 2009; Prikryl et al., 2015) and this is the focus of the present study.

181 Phase scintillation is commonly quantified by the standard deviation of the signal phase,
182 σ_{ϕ} , which is usually computed across 60 seconds. The refractive component of the signal is
183 usually assumed to be slowly varying and associated with frequencies of less than 0.1 Hz.
184 Therefore, by only considering frequencies greater than 0.1 Hz, the diffractive effects (usually
185 referred to as scintillation) can be distinguished (Fremouw et al., 1978). However, the 0.1 Hz

186 cutoff can give spurious observations of phase scintillation as a result of erroneous data
187 detrending (Forte and Radicella, 2002). When a GNSS satellite is observed at low elevation
188 angles the σ_ϕ index cannot distinguish between phase scintillation and background noise for
189 weak to moderate phase scintillation (Forte, 2005). Wang et al. (2018) showed that rapid
190 variations in the phase of a trans-ionospheric signal can arise as a result of plasma structures
191 moving rapidly relative to an observer at ground level, and so can give the appearance of
192 phase scintillation. Rapid changes in the spatial distribution of electron density can also
193 introduce similar effects as the GNSS satellite-to-receiver ray path can sweep through these
194 irregularities at high speed, resulting in high-frequency refractive variations (McCaffrey and
195 Jayachandran, 2019).

196 The presence or absence of scintillation effects on trans-ionospheric radio signals have been
197 extensively studied for electron density enhancements in the high-latitude ionosphere, but
198 the effect of the steep plasma density gradients at the edge of depletions, such as polar holes
199 are not as extensively studied. The purpose of this paper is to report on the effects of such
200 steep density gradients on GNSS signals, observed in three multi-instrument case studies
201 close to northern winter solstice, and to provide observational evidence which supports the
202 work of Aarons (1982).

203 **Instrumentation**

204 The European Incoherent Scatter Scientific Association (EISCAT) operates the EISCAT Svalbard
205 Radar (ESR) at Longyearbyen (78.2° N, 16.0° E; 15.2° MLAT, 112.9° MLON) on Svalbard
206 (Wannberg et al., 1997). The site consists of two antennas, a 32-meter parabolic dish and a
207 42-meter parabolic dish. The 42 m dish is fixed along the direction of the local geomagnetic
208 field lines (azimuth -179°; elevation 81.6°), while the 32 m dish is steerable in both azimuth
209 and elevation. Observations of the electron density, electron temperature, ion temperature,
210 and ion drift line of sight velocity in the ionosphere from this incoherent scatter radar (ISR)
211 are used in this study.

212 The Super Dual Auroral Radar Network (SuperDARN) is a network of high latitude coherent
213 scatter radars (Greenwald et al., 1995; Chisham et al., 2007; Nishitani et al., 2019) that observe
214 line-of-sight plasma velocities in the F-region. These measurements are assimilated using the
215 map potential technique (Ruohoniemi and Baker, 1998), which uses an ionospheric

216 convection model to map the electrostatic potential pattern. Electrostatic equipotential lines
217 are streamlines of ionospheric convection flows. As the plasma drift velocity is perpendicular
218 to both the electric and magnetic fields in the F-region ($\underline{E} \times \underline{B}$ drift) the plasma convection
219 pattern can be directly inferred from the electric potential maps.

220 GNSS signals detected by NovAtel GPStation-6 receivers at the Kjell Henriksen Observatory
221 (KHO) (78.2° N, 16.0° E; 15.2° MLAT, 112.9° MLON) can be used to infer the effects of the
222 ionosphere on radio waves traveling through this medium. Amplitude scintillation is measured
223 using the S_4 index, which is the square root of the variance of received power divided by the
224 mean value of the received power (Briggs and Parkin, 1963). Phase scintillation is measured
225 using the σ_ϕ index, which is the standard deviation of the detrended carrier phase ϕ in radians
226 (Fremouw et al., 1978) over 60 seconds.

227 The IMF was observed by the Advanced Composition Explorer (ACE), which is a NASA
228 Spacecraft orbiting the L1 Lagrangian point of the Earth Sun system, roughly 1.54 million km
229 from the Earth (Zwickl et al., 1998). In addition to the x-, y- and z- components of the IMF the
230 clock angle, given by $\arctan \frac{|B_y|}{|B_z|}$, is also considered. When the clock angle is greater than 45
231 degrees either $|B_y| > |B_z|$ or $B_z < 0$, in either case a two cell convection pattern is expected with
232 antisunward flow drawing plasma from day to night across the polar cap (Thomas and
233 Shepherd, 2018).

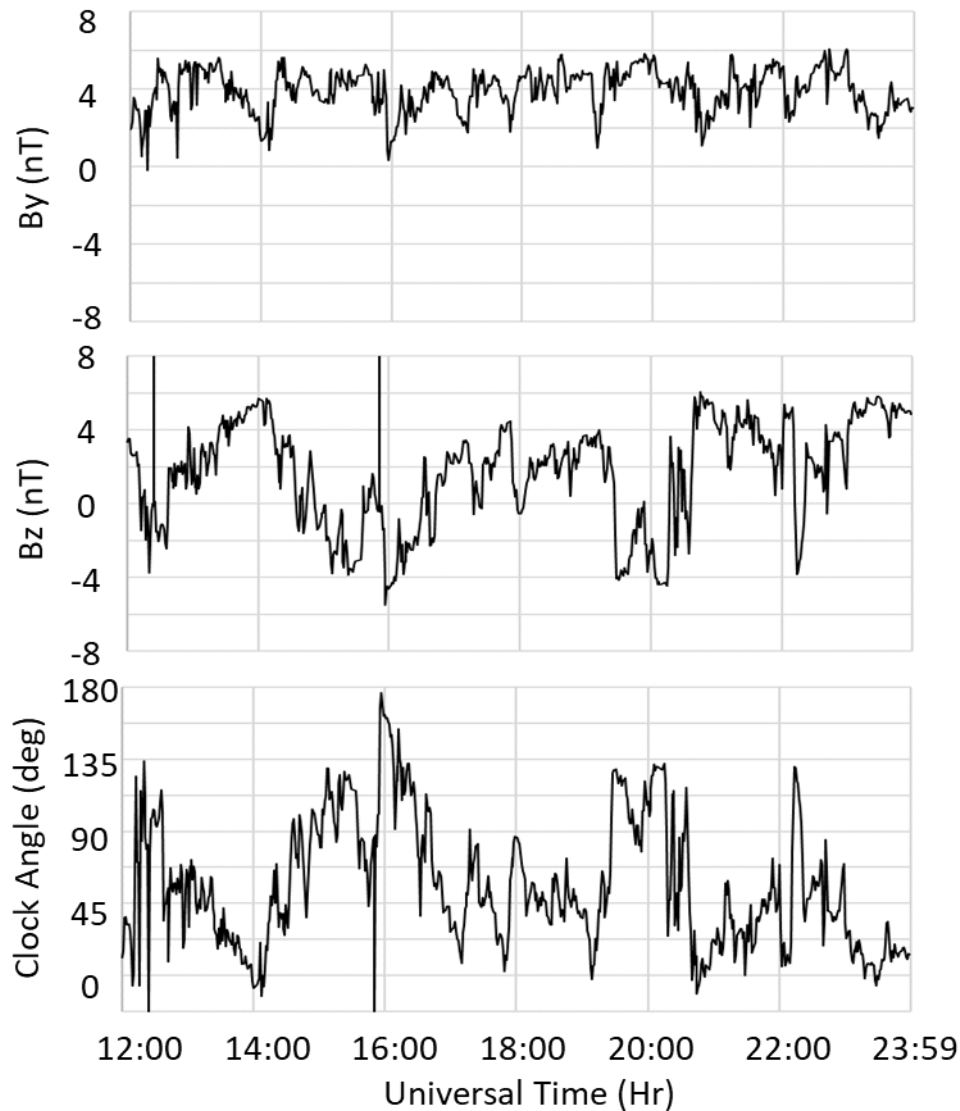
234 Total Electron Content (TEC) maps are used to put these measurements into context. These
235 were obtained from the Madrigal Database at the MIT Haystack Observatory (Ridout and
236 Coster, 2006; Vierinen et al., 2015). Two other indices are used within this study. The K_p index
237 is used as a proxy for disturbances to the geomagnetic field. The F10.7 cm solar flux is used as
238 a proxy for solar activity. These indices were both obtained from the UK Solar System Data
239 Centre (UKSSDC) at Rutherford Appleton Laboratory, UK.

240 **Results**

241 **Case study: 17th December 2014**

242 The 3-hourly K_p values observed on 17th December 2014 between 12:00 and 23:59 UT ranged
243 between 1- and 1+, indicating quiet conditions. The F10.7 cm solar flux was relatively high,

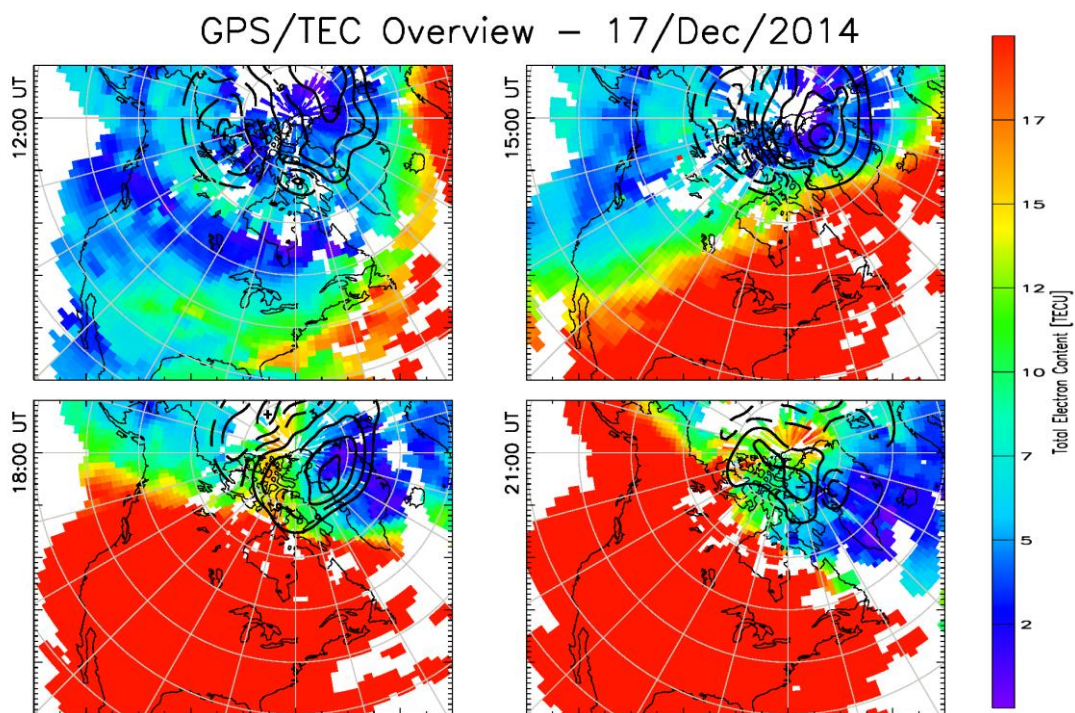
244 the value of 198.5 sfu is typical of solar maximum. The IMF observed by the ACE spacecraft
245 between 12:00 and 23:59 UT (Fig. 1) was characterised by a positive value for the IMF B_y (mean
246 value 3.9 nT). IMF B_z was more variable, but generally took smaller values (mean value of 1.7
247 nT). The clock angle was generally greater than 45° from 14 UT until 19 UT, and the
248 corresponding SuperDARN plots (discussed later in this section) show that a two cell
249 convection pattern dominated until at least 20 UT.



250

251 **Fig. 1.** The y - and z -components of the IMF, and the clock angle observed by the ACE
252 spacecraft between 12:00 UT and 23:59 UT on 17th December 2014. The data have been time
253 shifted to the nose of the Earth's bow shock.

254 Total Electron Content (TEC) maps (Fig. 2) show the overall plasma density throughout the
 255 high-latitude regions. The TEC maps at 12 UT and 15 UT show values of ~ 2 TECu (dark blue
 256 colour) in the polar cap. At 18 UT at 21 UT larger electron densities can be observed crossing
 257 the polar cap in a two cell convection pattern, with values of ~ 15 TECu (yellow colour),
 258 indicating that plasma produced by photoionisation on the dayside is being drawn into the
 259 polar cap. This plasma is being drawn into the polar cap during relatively quiet conditions
 260 ($K_p \sim 1$) and is consistent with a two cell convection pattern.



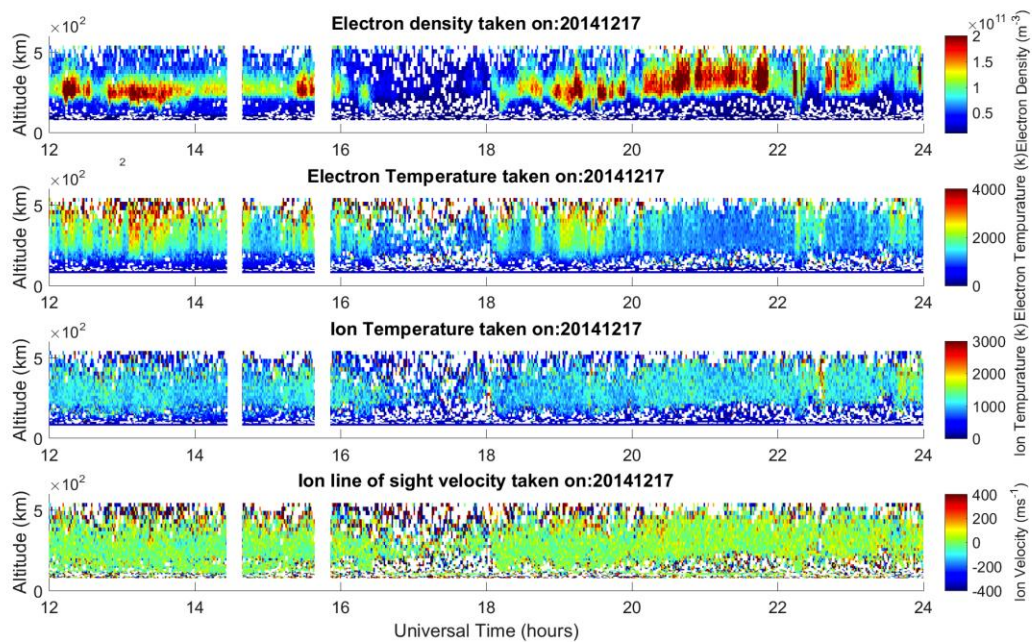
261

262 **Fig. 2. TEC maps for the 17th December 2014 extrapolated from TEC collected by a network**
 263 **of GNSS receivers at three hourly intervals between 12 UT and 21 UT.**

264 The electron densities and temperatures observed by the field-aligned 42 m dish of the EISCAT
 265 Svalbard Radar (ESR) between 12:00 UT and 23:59 UT are shown in Fig. 3. The scales on this
 266 plot have been chosen to enable a clear comparison with other figures presented in this
 267 paper. A clear depletion in the electron densities is observed between approximately 16 and
 268 18 UT at all altitudes. The electron and ion temperatures are not elevated at this time with
 269 values of approximately 1000 K, suggesting that this depletion is void of particle precipitation
 270 and did not arise from enhanced recombination due to Joule heating. The ESR does not show
 271 a substantial plasma velocity aligned with the radar beam. This radar observed at an elevation

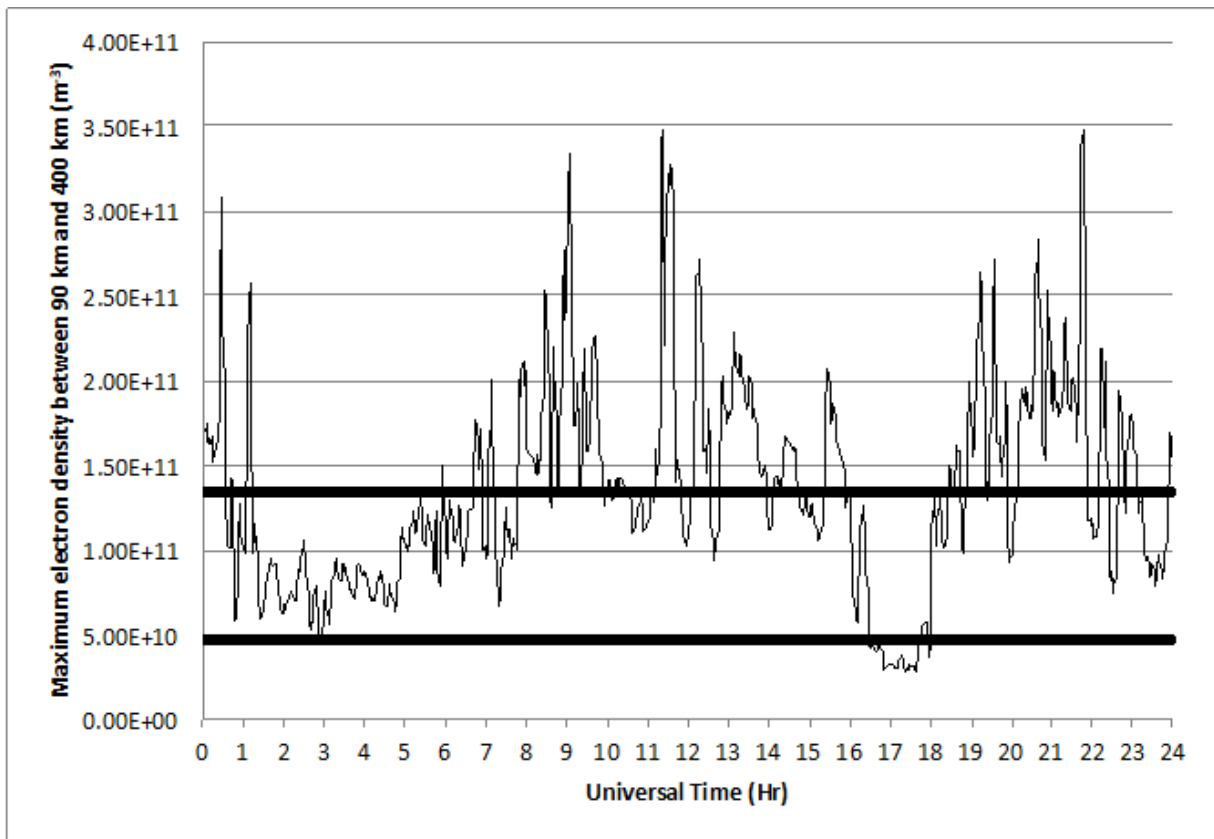
272 of 81.6° which is aligned with the magnetic field line in the F-region. There was no substantial
 273 component of velocity observed along the magnetic field line. In order to further investigate
 274 the electron density depletion, a line plot of the maximum detected electron density from 90-
 275 400 km is shown (Fig. 4). In addition to the maximum density two other values are present on
 276 the plot, the average value for the whole day, and 35% of the average value. The depletion
 277 was defined as when the electron density dropped below the 35% line and, in this case, the
 278 depletion was defined as starting at 16:29 UT and ending at 18:00 UT.

279



280

281 **Fig. 3. Electron densities, electron temperatures, ion temperatures, and ion drift line of sight**
 282 **velocity measured by the 42 m dish of the ESR observing at an azimuth of 184.5° and an**
 283 **elevation of 81.6° between 12:00 UT and 23:59 UT on 17th December 2014.**



284

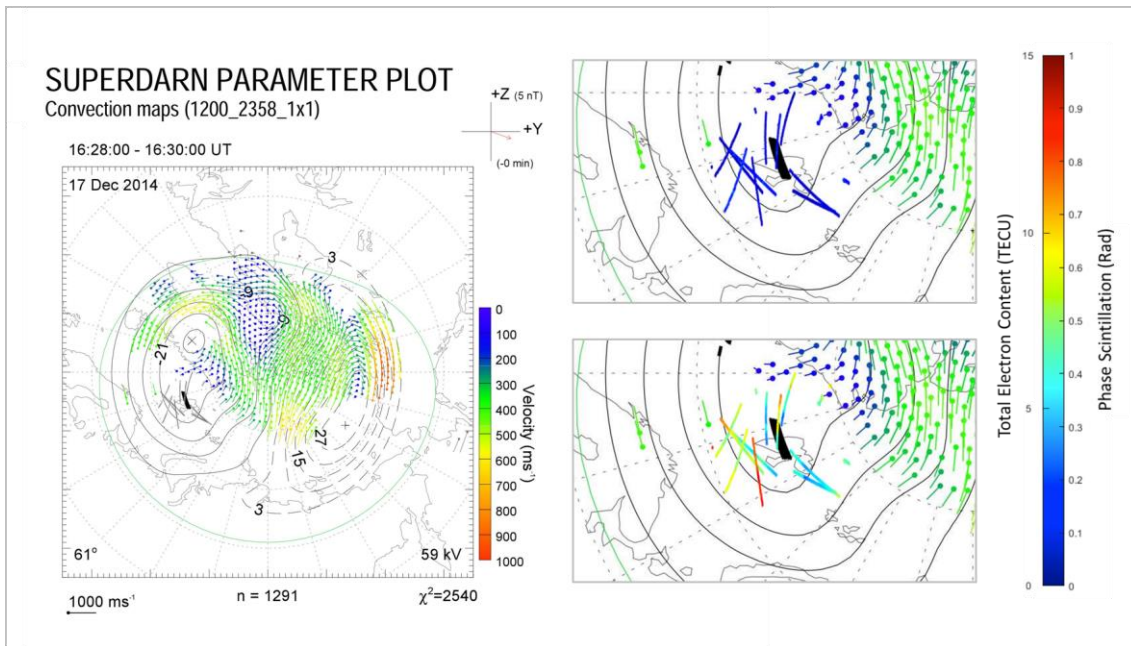
285 **Fig. 4. Maximum electron density between 90 and 400 km for ESR 42 m observation on the**
 286 **17th December 2014 at one minute resolution. A five point running mean was applied to**
 287 **these data. The upper horizontal line is the average value and the lower horizontal line is**
 288 **35% of the average. A hole can be seen between 16:29 and 18:00 UT.**

289 Fig. 5 shows the high-latitude convection pattern inferred from the SuperDARN radars for
 290 three representative times during the time that the electron density depletion was observed
 291 by the ESR. These clearly show a two cell convection pattern, with plasma drawn antisunward
 292 across the polar cap. The ESR observes at a given location, which rotates under the convection
 293 pattern. The depletion, identified in Fig. 4, is indicated by a black line. At midwinter Svalbard
 294 is in perpetual darkness. On 14th December the ground level terminator is at a maximum
 295 latitude of 68° N, which corresponds to a maximum magnetic latitude of 76° MLAT at 21 UT.
 296 This depletion is nightward of the terminator and the SuperDARN convection patterns suggest
 297 that this plasma is circulating in perpetual darkness. It is interpreted as a polar hole.

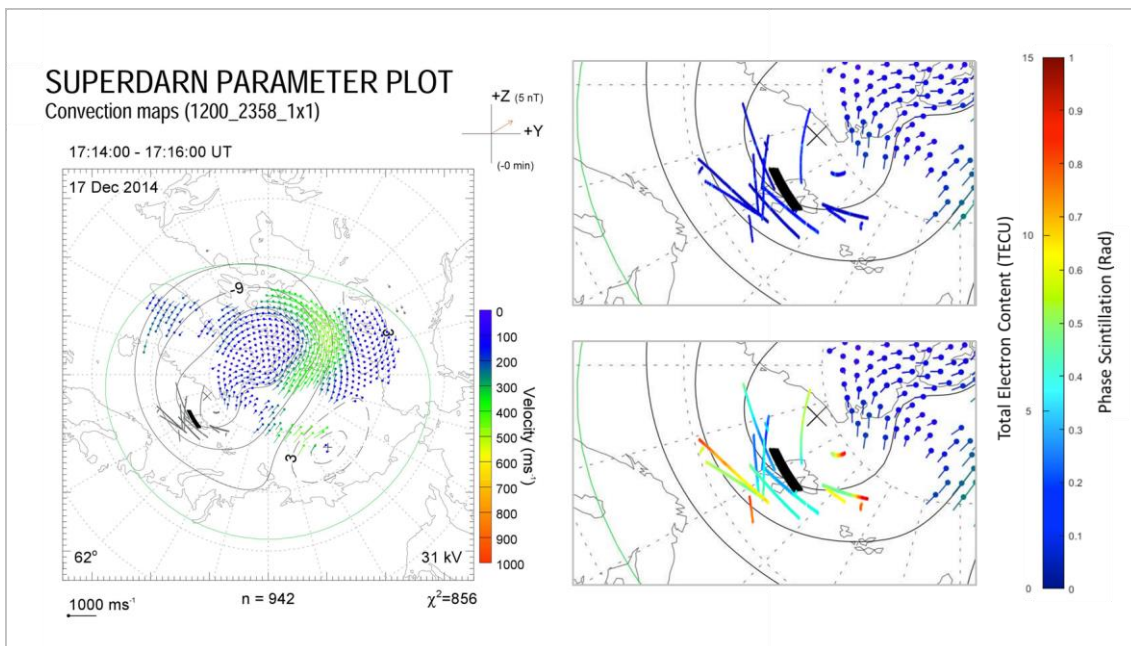
298

299

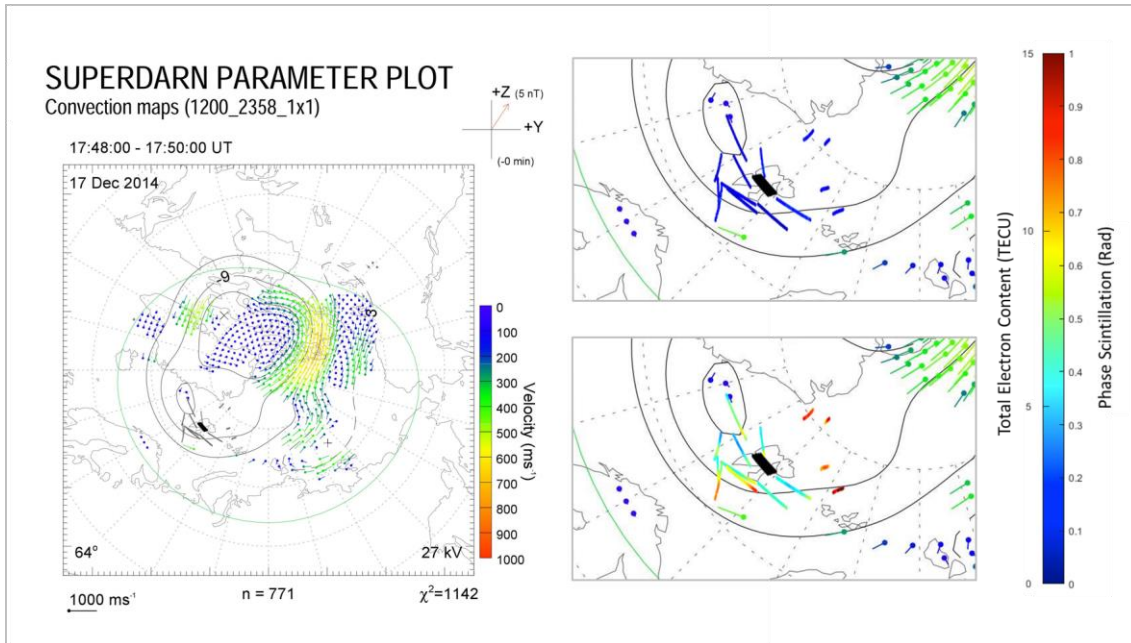
300



301



302



303

304 **Fig. 5. Electric potential patterns inferred from the SuperDARN radars for 16:28 UT, 17:14**
 305 **UT, and 17:48 UT on 17th December 2014 as a function of geomagnetic latitude and magnetic**
 306 **local time. Magnetic noon is at the top of each plot with dusk and dawn on the left- and**
 307 **right- hand sides respectively. Magnetic latitude is indicated by the grey dashed circular lines**
 308 **in 10.0° increments. The grey lines show the location of satellite passes from GNSS satellites,**
 309 **assuming an ionospheric intersection of 350 km. The SuperDARN plot from 16:28 UT includes**
 310 **satellite passes from 16:00-16:58 UT, the 17:14 UT plot includes satellite passes from 16:58-**
 311 **17:28 UT, and the 17:48 UT plot includes satellite passes from 17:28-18:02 UT. These time**
 312 **intervals were chosen as inspection of the whole SuperDARN data set at two minute**
 313 **resolution indicated that the convection patterns were relatively stable during these**
 314 **intervals. The right hand side of the panels show the area around the satellite passes in more**
 315 **detail. The multi-coloured colours represent phase scintillation (upper panel in each pair)**
 316 **and TEC (lower panel in each pair). The thick black line indicates the position of the polar**
 317 **hole observed with the 42 m dish of the EISCAT Svalbard Radar.**

318 The data collected by the GNSS receiver was from the GPS, Galileo and GLONASS systems and
 319 the receiver provides the azimuth and elevation of the satellite with respect to the receiver.
 320 This was converted into a latitude and longitude using the radio wave path and assuming that
 321 the data corresponds to 350 km in altitude, in line with previous studies (e.g. Cervera and
 322 Thomas, 2006; Forte and Radicella, 2002). At low elevation angles the GNSS TEC and
 323 scintillation data can become unreliable due to multi-path issues, so observations at an

324 elevation of less than 30° were discarded. This cut of has been used in previous studies, for
325 example Mitchell et al. (2005). Signal lock times below 240 seconds were also discarded, in
326 line with previous studies (e.g. van der Meeren et al., 2015). The satellite tracks were overlaid
327 onto SuperDARN plots. (Fig. 5)

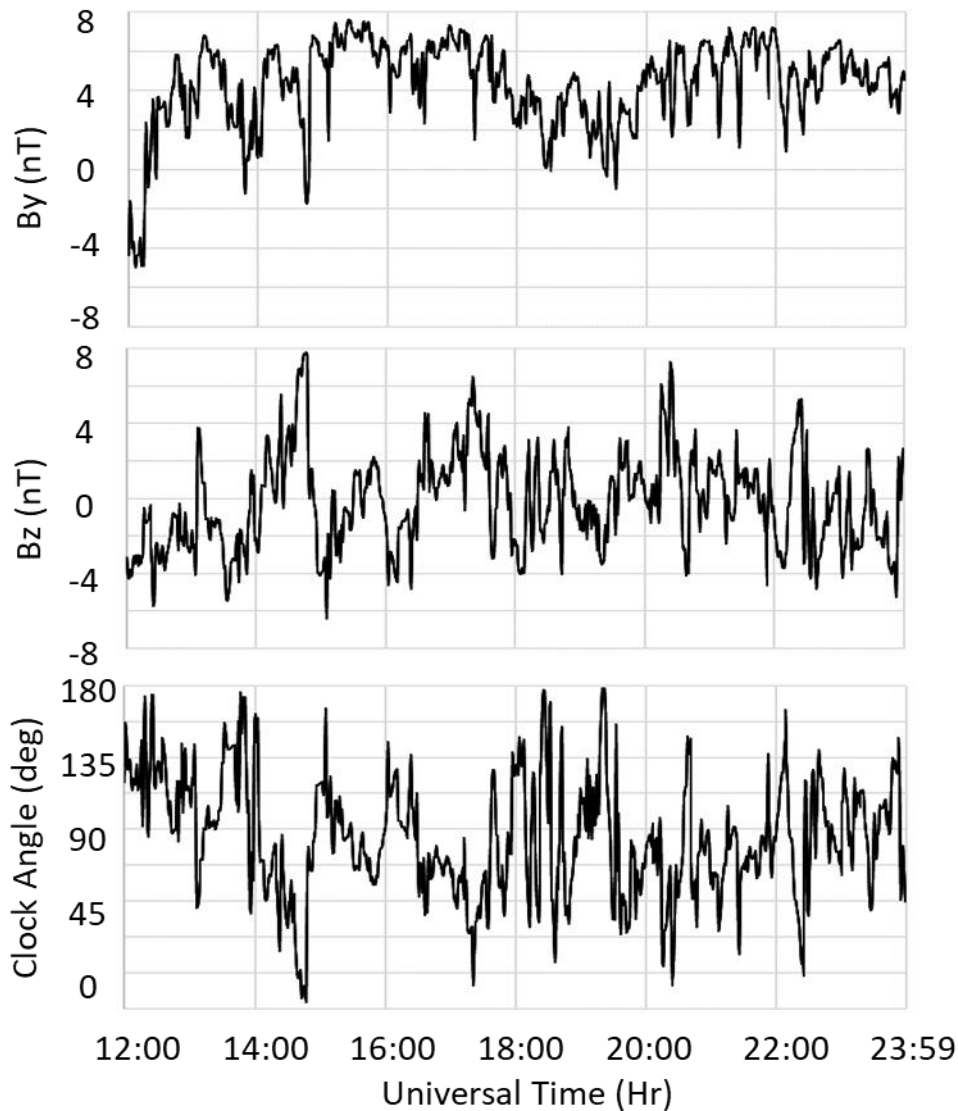
328 TEC and phase scintillation data from GNSS receivers were taken during times when the polar
329 hole was observed. This hole is observed for 1.5 hours and several satellite paths are present
330 during this time window. The GNSS TEC data clearly show lower TEC levels at and around the
331 area marked by the ESR as a hole and, on some of the satellite trajectories, sharp changes can
332 be seen with the edge of the hole. A one-to-one correspondence between the GNSS TEC data
333 and the EISCAT data is neither expected or observed. It is highly likely that the polar hole will
334 evolve during the time for which it is observed, and therefore the plots in figure 5 include both
335 spatial and temporal variation. The ESR observes the polar hole for 91 minutes and the plasma
336 velocity inferred from the electric potential patterns inferred from the SuperDARN radars
337 (figure 5) at this location is of the order of 150 m s^{-1} , indicating that the polar hole has a
338 horizontal extent of some 800 km in a direction parallel to the plasma flow. In summary the
339 combination of the EISCAT and GNSS TEC measurements indicate that the polar hole is present
340 for an extended period of time (of the order of hours) over a large (hundreds of km) spatial
341 scale.

342 Panels showing the location of phase scintillation on the satellite tracks are also shown in
343 figure 5. A threshold of 0.2 rad was used to identify phase scintillation. Different authors have
344 used different thresholds for phase scintillation, including 0.2 rad (e.g. van der Meeren, 2015),
345 0.25 rad (e.g. Alfonsi et al., 2011) and 0.3 rad (e.g. Kinrade et al., 2013). The purpose of using
346 a low threshold within the present study was to ensure that any possible indication of phase
347 scintillation was included. Since TEC and scintillation are collected simultaneously, comparing
348 the two might be expected to show increased scintillation where there are changes in TEC.
349 No scintillation was observed on the edges of the holes.

350 **Case study 2: 10th December 2015**

351 The F10.7cm solar flux for this case was lower than in the first study, with a value of 108.5 sfu.
352 The K_p index was higher, with a value of 3 from 12 to 18 UT and a value of 4 at 21 and 24 UT,
353 indicating an active state, but not storm levels. Once again the IMF was variable, with B_z taking

354 positive and negative values. B_y was consistently larger than B_z and dominated. As in the
355 previous case study a two cell convection pattern was observed.



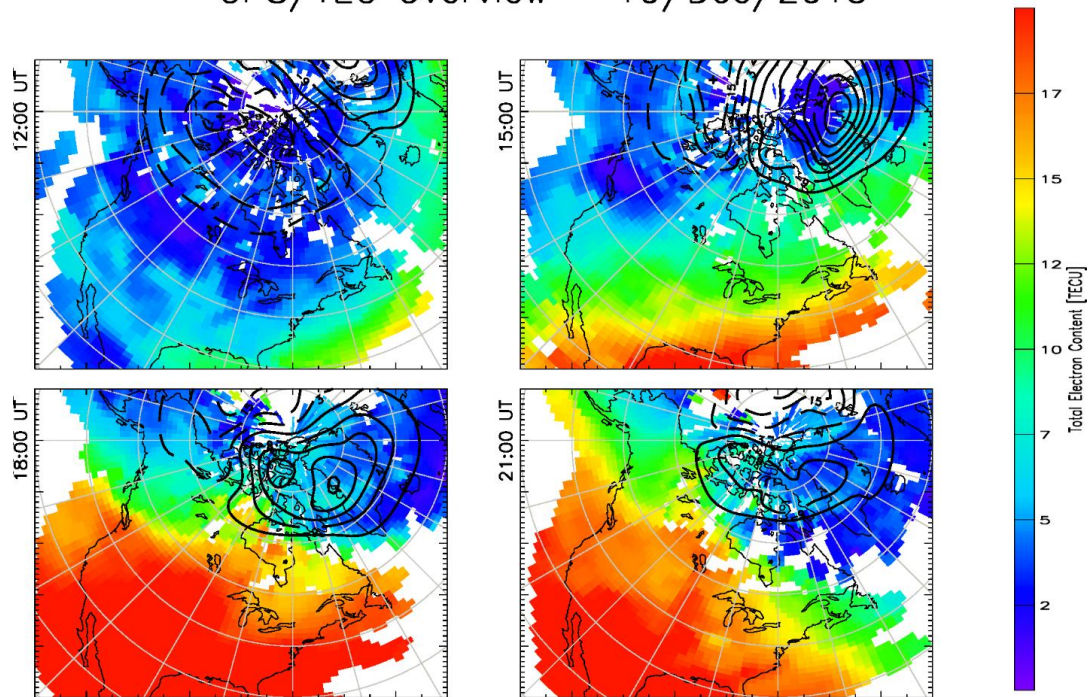
356

357 **Fig. 6. The y- and z-components of the IMF, and the clock angle observed by the ACE**
358 **spacecraft between 12:00 and 23:59 UT on 10th December 2015, in the same format as Fig.**
359 **1. The data have been time shifted to the nose of the Earth's bow shock.**

360

361 The TEC maps at 18 and 21 UT are shown in Fig. 7. As in the previous case study these indicate
362 higher density plasma produced at lower latitudes being drawn across the polar cap within
363 the high latitude convection pattern, with this effect maximising at 21 UT.

GPS/TEC Overview – 10/Dec/2015

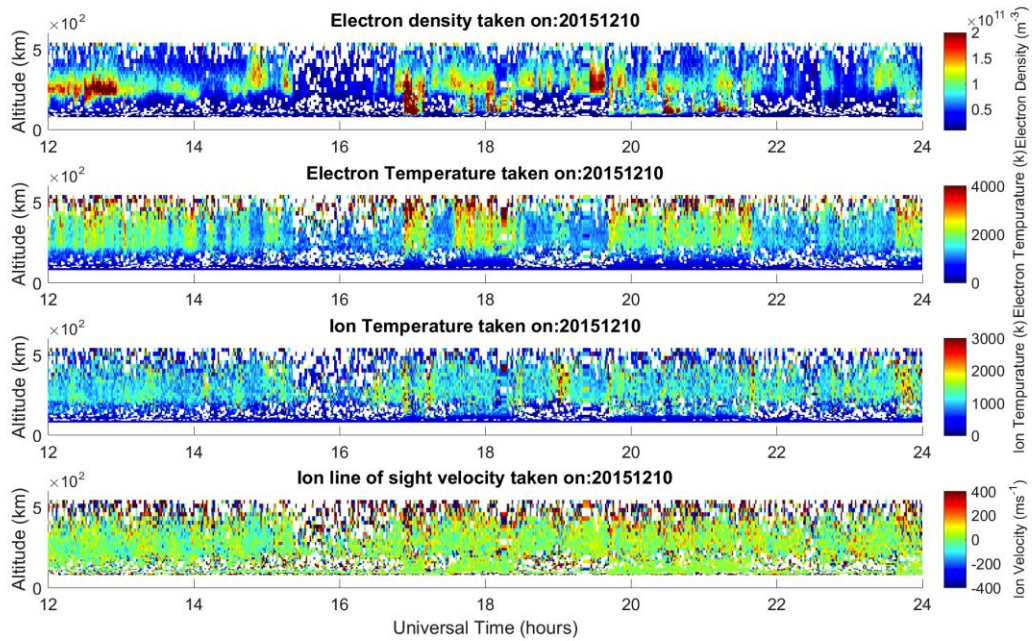


364

365 **Fig. 7. TEC maps for the 10th December 2015 extrapolated from TEC collected by a network**
366 **of GNSS receivers at three hourly intervals between 12 and 21 UT.**

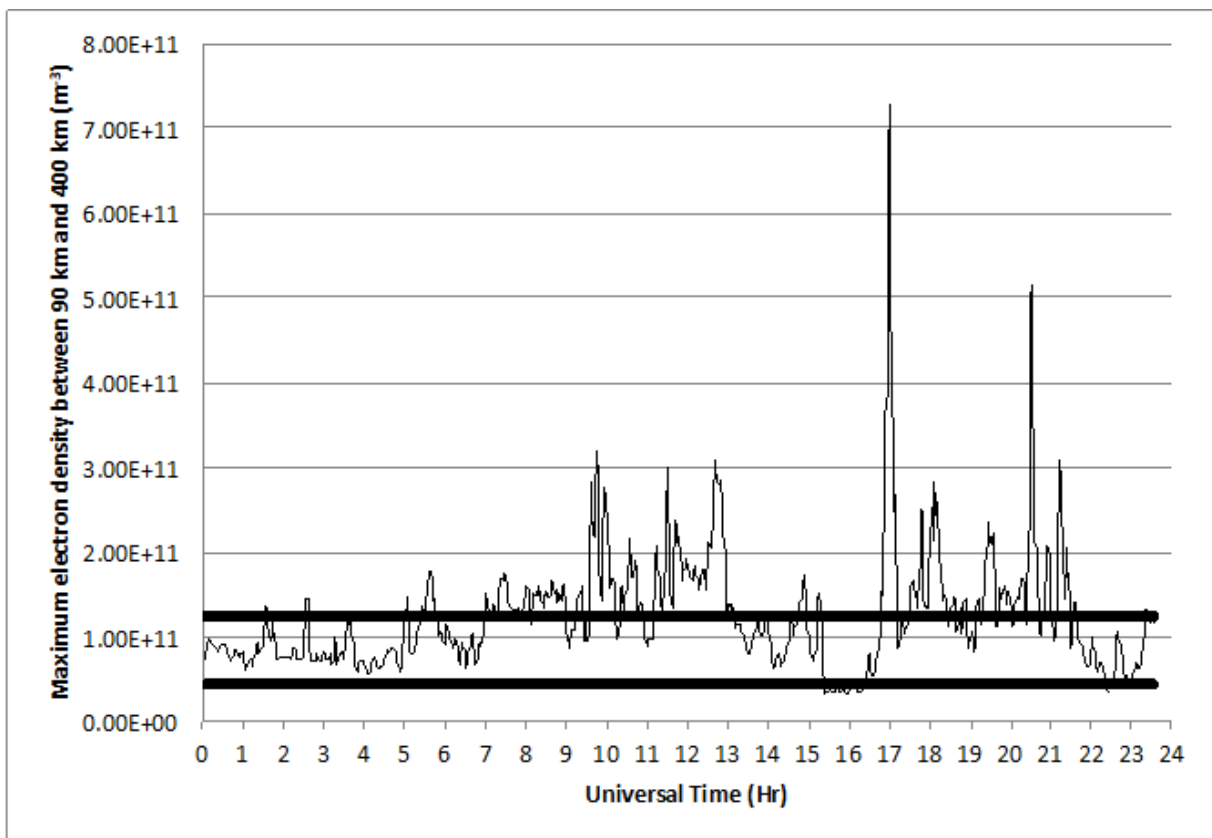
367 The 42 m ESR observations (Fig. 8) for this day show an electron density depletion that
368 contains all the previously discussed markers, with no significant velocity in the field aligned
369 direction.

370 Using the same method as in the previous case the hole was identified, with the start and
371 end times given as 15:15 and 16:43 UT. The 32 m ESR observations (Fig. 15) show a depletion
372 at around 15 UT.



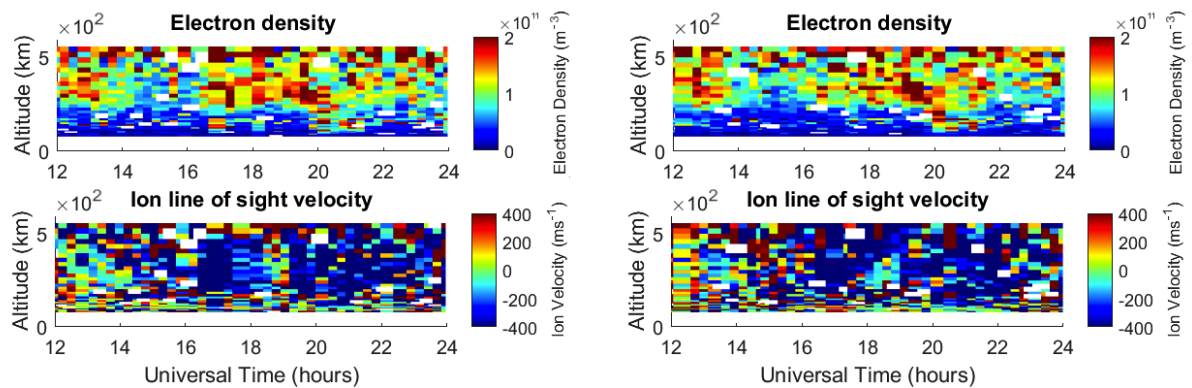
373

374 **Fig. 8. Electron densities, electron temperatures, ion temperatures, and ion drift line of sight**
 375 **velocity measured by the 42 m dish of the ESR observing at an azimuth of 184.5° and an**
 376 **elevation of 81.6° between 12:00 and 23:59 UT on 10th December 2015.**



377

378 **Fig. 9. As Fig. 4 but for 10th December 2015. A polar hole can be seen between 15:24 and**
 379 **16:25 UT.**



380

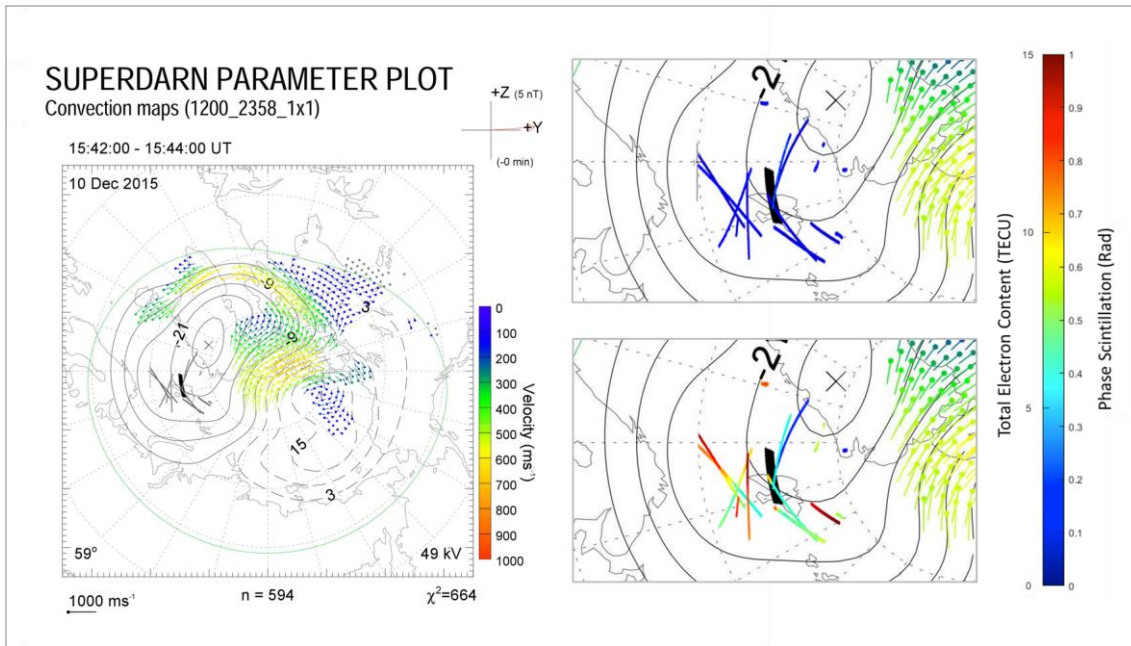
381 **Fig. 10. Electron densities and ion drift line of sight velocities observed by the 32 m dish of**
 382 **the ESR at -43° azimuth and 30° elevation (left hand side) and at -14° azimuth and 30°**
 383 **elevation (right hand side) between 12:00 and 23:59 UT on 10th December 2015.**

384 The high-latitude convection pattern was inferred from the SuperDARN radars (Fig. 11), with
 385 the location of the polar hole observed in the 42 m ESR observations, and GNSS TEC and phase
 386 scintillation measurements overlaid as in the previous case study. The 32 m ESR observations
 387 (Fig. 9) were directed poleward; indicating that this is a polar hole rather than the ionospheric
 388 trough, which would be located equatorward of the radar. A substantial plasma velocity of
 389 some 300 m s^{-1} towards the radar was observed at 16:00 UT, indicating cross-polar flow in the
 390 equatorward direction. The high-latitude convection pattern inferred from the SuperDARN
 391 radars also shows antisunward cross-polar flow, but with a more asymmetric convection
 392 pattern than was observed on 17th December 2014. On 10th December 2015 there was a clear
 393 dominant dusk cell, drawing plasma across the polar cap from the pre-noon sector. The polar
 394 hole observed with the 42 m dish of the ESR was in the sunward return flow in the dusk
 395 convection cell.

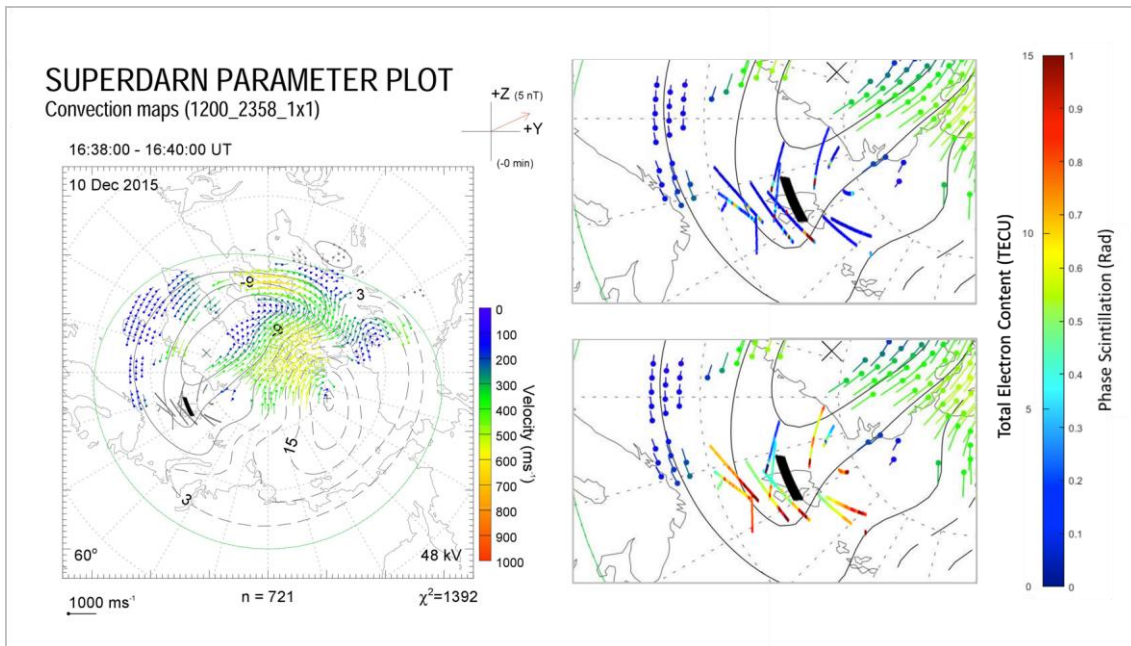
396 The phase scintillation plot for 15:16 to 16:14 UT (upper right panel of Fig. 11) has some
 397 satellite trajectories passing through the hole boundary, but displays no significant
 398 scintillation on any of the paths. The later plot (second panel from the bottom on the right
 399 panel of Fig. 11) does contain phase scintillation seen however none of the elevated
 400 scintillation matches up to hole boundaries, instead, the scintillation is seen in regions of high
 401 and elevated electron density.

402

403



404



405

406 **Fig. 11. Electric potential patterns inferred from the SuperDARN radars for 15:42 UT and**
407 **16:38 UT on 10th December 2015, with data from GNSS satellites overlaid in the same format**
408 **as Fig. 5. The intervals for which the satellite passes were plotted are from 15:16-16:14 UT**
409 **(15:42 UT plot) and from 16:14-17:04 UT (16:38 UT plot).**

410

411 **Discussion**

412 A series of polar ionospheric holes have been detected in the high latitude nightside
413 ionosphere in case studies close to winter solstice, under varying solar intensities and
414 geomagnetic disturbance levels. The first study on 17th December 2014 was characterised by
415 high levels of solar activity (198.5 sfu) and quiet geomagnetic conditions. The second case
416 study, on 10th December 2015 also had lower levels of solar activity of (108.5 sfu), but had
417 more active geomagnetic conditions ($K_p=3$) than in the previous study. A third case study,
418 under quiet geophysical conditions ($K_p\leq 2$) and moderate solar activity (F10.7 cm solar flux =
419 116.7 sfu) on 12th December 2015 showed similar results (not shown).

420 Ionospheric polar holes contain much lower electron densities than those detected through
421 the rest of the day, this study used the maximum density at a given time dropping 35% below
422 the daily average maximum density to identify these holes. The changes in electron density
423 are associated with large electron density gradients. Table 1 shows the electron density
424 gradients and average hole electron density, based on observations from the ESR 42 m. The
425 average polar hole density observed in this study is comparable to those previously reported
426 of 10^8 - 10^{11} electrons·m⁻³ (Obara and Oya, 1989, Benson and Grebowsky, 2001). Steep electron
427 density gradients are observed at the edges of the holes, these are expressed in units of
428 $\Delta N_e \cdot m^{-3} \cdot h^{-1}$. Although these gradients are expressed in units of h⁻¹ they were calculated from
429 successive observations by the ESR 42 m (these measurements are typically one minute
430 apart). The spatial extent of these holes was at least several hundred kilometres, as inferred
431 from the GNSS TEC measurements (all studies) and the ESR 32 m observations (case study
432 from 17th December 2014). Polar holes are usually associated with quiet geomagnetic
433 conditions ($K_p < 2$). It is notable that, on 10th December 2015, a polar hole was observed under
434 more active geomagnetic conditions ($K_p=3$).

Date	1 st Edge $\Delta N_e \cdot m^{-3} \cdot h^{-1}$	2 nd Edge $\Delta N_e \cdot m^{-3} \cdot h^{-1}$	Average Hole $N_e \cdot m^{-3}$
17/12/2014	1.0E+11	0.91E+11	0.40E+11
10/12/2015	3.5E+11	1.6E+11	0.22E+11
12/12/2015	0.79E+11	1.0E+11	0.18E+11

Table 1 – The electron density gradient at each edge of the polar hole and the average electron density inside the hole at 350 km observed by ESR 42 m.

435

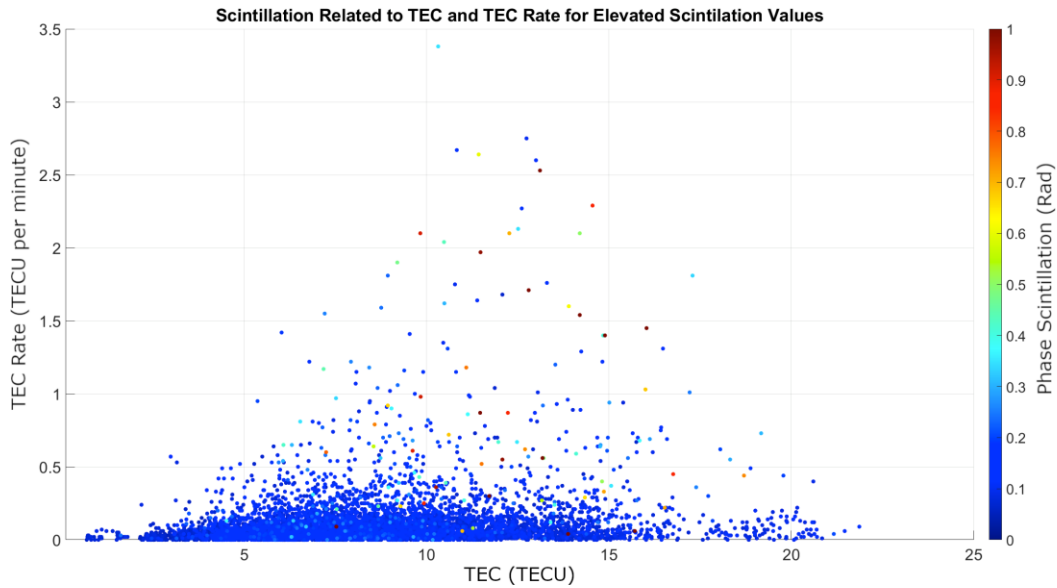
436 The IMF conditions during the time when the polar holes were observed, and for several hours
437 beforehand, were appropriate for antisunward cross-polar convection. The ground level solar
438 terminator for winter is only above 70° MLAT between 15 UT and slightly after 21 UT, reaching
439 a maximum latitude of just under 76° MLAT on the dayside at around 21 UT, creating the
440 possibility that plasma within the high-latitude convection pattern could circulate in perpetual
441 darkness, thus undergoing recombination whilst simultaneously being insulated from
442 photoionisation, or precipitation, creating a polar hole.

443 Phase scintillation has previously been observed to coincide with large plasma gradients such
444 as on the edge of ionospheric enhancements such as polar cap patches (Jin et al., 2017), the
445 tongue of ionisation (van der Meeren et al., 2014), plasma structures associated with the
446 aurora (Kinrade et al., 2013; Oksavik et al., 2015; van der Meeren et al., 2015) and the mid-
447 latitude trough (Pryse et al., 1991). The structures that cause scintillation arise due to the
448 Gradient Drift Instability and/or the Kelvin Helmholtz Instability (Keskinen and Ossakow, 1983;
449 Carlson et al., 2008). In the present study, once the boundaries and the large electron density
450 gradients associated with them were identified, these boundaries were investigated for
451 elevated levels of phase scintillation. A threshold of 0.2 rad was used, the purpose of this low
452 value was to ensure that any possible indication of phase scintillation was included. Across all
453 of the observed GNSS points coinciding with the polar hole boundaries no such levels of phase
454 scintillation were detected. Phase scintillation usually dominates at high latitude (e.g., Prikryl
455 et al., 2015), although amplitude scintillation has also been observed (e.g. Mitchell et al.,
456 2005). The present study focuses upon phase scintillation as no amplitude scintillation,
457 defined as when the S4 index was greater than 0.2, was observed on any of the TEC gradients
458 at the boundaries of the polar holes.

459 This is not the first time a plasma density enhancement has been observed without
460 corresponding phase scintillation. Van der Meeren et al. (2016) observed a Sun-aligned polar
461 cap arc under quiet geomagnetic conditions without corresponding scintillation. In the
462 present study some phase scintillation was observed, however, these points coincide with
463 increases in TEC and the edges of spikes in electron densities at other locations. In the second
464 case study (10th December 2015) phase scintillation was observed at a point associated with
465 elevated TEC (lower right panels of Fig. 11), but this was not associated with the assumed
466 boundary of the polar hole.

467 When phase scintillation was observed it was always associated with electron density
468 gradients, but converse is not always true. Therefore it appears that some minimum level of
469 overall electron density is needed for phase scintillation to occur. Given that it is the presence
470 of small scale structures that cause scintillation, this suggests that these small scale structures
471 have not arisen.

472 Figure 12 shows phase scintillation as a function of TEC and TEC rate of change. This figure
473 also includes data from a third study, using data from 12th December 2015, which was
474 consistent with the interpretation presented here, but which has been omitted in the interest
475 of concision. Low scintillation can be seen at all TEC levels and for a majority of the range of
476 TEC rates of change. On the other hand, elevated scintillation levels are only seen above
477 approximately 6 TECU suggesting that a minimum electron density is required. This is not a
478 new idea, in his review paper Aarons (1982) commented 'if the ionosphere is perturbed on a
479 percentage basis, *change in N* in the trough will be small since *N* is low; scintillations will then
480 be low.' The current paper provides observational evidence to support this suggestion that a
481 minimum electron density is required. The current paper is also consistent with suggestions
482 made by Prikryl et al. (2015), where the strongest phase scintillations were found to be highly
483 collocated with regions that are ionospheric signatures of the coupling between the solar
484 wind and magnetosphere. Polar holes appear to be areas of weak coupling, hence less
485 scintillation.



486

487 **Fig. 12 – Phase scintillation as a function of TEC and the TEC rate of change per minute for**
 488 **17th December 2014, 12th December 2015 and 10th December 2015.**

489 In this study the phase scintillation index (σ_ϕ) has been calculated across a 60 second interval,
 490 in line with common practice within this field. However, if this index was computed across a
 491 shorter time interval, then it is possible that elevated values of σ_ϕ may be associated with the
 492 edge of the polar hole. This would be an interesting topic for a future paper. Further
 493 developments upon this work would expand the observations of the polar holes discussed to
 494 a larger number of examples under a wider range of geophysical conditions. Polar ionospheric
 495 holes could be tracked by making observations with a higher temporal resolution at a large
 496 number of regularly spaced locations. The advent of EISCAT-3D (McCrea et al., 2015), which
 497 will give unprecedented temporal and spatial coverage, will enable such studies in the
 498 European sector of the high-latitude ionosphere. The ability to observe the evolution of polar
 499 holes over time will give a new, deeper, understanding of these features and how they
 500 influence practical radio systems such as GNSS.

501 **Conclusions**

502 Polar ionospheric holes are regions of electron density depletions containing large electron
 503 density gradients at their boundaries. This paper reports case study observations of polar
 504 ionospheric holes conducted using the ESR and GNSS receivers. These holes were observed
 505 during both quiet and moderately disturbed geomagnetic conditions, under a range of solar

506 activities. Steep electron density gradients have been associated with phase scintillation at
507 GNSS frequencies in previous studies, however no enhanced scintillation was detected upon
508 the electron density gradients at these boundaries. Phase scintillation was only observed
509 when electron density levels were elevated above 6 TECU. Aarons (1982) suggested that a
510 minimum density level may be required for scintillation to occur, and the present study
511 provides supporting observational evidence. We conclude that both a minimum electron
512 density level and a sharp gradient in the electron density must be present for instability
513 mechanisms to produce scintillation structures.

514 **Author contribution**

515 This work was led by Luke Jenner, under the guidance of Alan Wood. Kjellmar Oksavik provided
516 the GNSS TEC and scintillation data, together with guidance regarding their interpretation. Tim
517 Yeoman and Alexandra Fogg provided the SuperDARN electric potential maps, together with
518 guidance regarding their interpretation. Anthea Coster provided the TEC maps, together with
519 guidance regarding their interpretation. All authors contributed to the discussion. The
520 manuscript was prepared by Luke Jenner and Alan Wood.

521 **Competing interests**

522 The authors declare that they have no conflict of interest.

523 **Acknowledgements**

524 EISCAT is an international facility supported by the national science councils of China, Finland,
525 Japan, Norway, Sweden, and the United Kingdom. The assistance of Ingemar Häggström and
526 colleagues at the EISCAT Scientific Association in running the experiments is gratefully
527 acknowledged. The data used in this paper is publicly available at <https://www.eiscat.se>. The
528 assistance of Steve Crothers and Matthew Wild at Rutherford Appleton Laboratory with the
529 data processing is gratefully acknowledged. The GNSS TEC and scintillation data were provided
530 by Kjellmar Oksavik at the University of Bergen, and is supported by the Norwegian Research
531 Council under contracts 212014 and 223252. The authors acknowledge the use of SuperDARN
532 data, data for which is available at <https://vt.superdarn.org>. SuperDARN is a collection of

533 radars funded by national scientific funding agencies of Australia, Canada, China, France, Italy,
534 Japan, Norway, South Africa, United Kingdom and the United States of America.' Alexandra
535 Fogg is supported by a studentship from the Science and Technology Facilities Council (UK).
536 The assistance of Nathan Brown with the production of Fig. 5 and Fig. 11 is gratefully
537 acknowledged. GPS TEC data products and access through the Madrigal distributed data
538 system are provided to the community (<http://www.openmadrigal.org>) by the Massachusetts
539 Institute of Technology (MIT) under support from US National Science Foundation grant AGS-
540 1242204. Data for TEC processing is provided from the following organizations: UNAVCO,
541 Scripps Orbit and Permanent Array Center, Institut Geographique National, France,
542 International GNSS Service, The Crustal Dynamics Data Information System (CDDIS), National
543 Geodetic Survey, Instituto Brasileiro de Geografia e Estatística, RAMSAC CORS of Instituto
544 Geográfico Nacional de la República Argentina, Arecibo Observatory, Low-Latitude
545 Ionospheric Sensor Network (LISN), Topcon Positioning Systems, Inc., Canadian High Arctic
546 Ionospheric Network, Centro di Ricerche Sismologiche, Système d'Observation du Niveau des
547 Eaux Littorales (SONEL), RENAG : REseau NATional GPS permanent, GeoNet - the official source
548 of geological hazard information for New Zealand, GNSS Reference Networks, Finnish
549 Meteorological Institute, and SWEPOS - Sweden. Access to these data is provided by madrigal
550 network via: <http://cedar.openmadrigal.org/>. The K_p index and F10.7 cm solar flux were
551 obtained from the UK Solar System Data Centre at Rutherford Appleton Laboratory. These can
552 be accessed at <https://www.ukssdc.ac.uk/>. The IMF data were provided by N. Ness and
553 obtained from the CDAWeb at <https://cdaweb.gsfc.nasa.gov/>.

554

555 **References**

556 Aarons, J.: Global Morphology of Ionospheric Scintillations, Proceedings of the IEEE, 70, 4,
557 360-378, doi: 10.1109/PROC.1982.12314, 1982.

558 Alfonsi, L., Spogli, L., De Franceschi, G., Romano, V., Aquino, M., Dodson, A., and Mitchell C.
559 N.: Bipolar climatology of GPS ionospheric scintillation at solar minimum, Radio Sci. , 46,
560 RS0D05, doi:10.1029/2010RS004571, 2011.

561 Anderson, D. N., Buchau, J., and Heelis R. A.: Origin of density enhancements in the winter
562 polar cap ionosphere, Radio Sci., 23, 513-519, doi: 10.1029/RS023i004p00513, 1988.

563 Benson, R., and Grebowsky, J.: Extremely low ionospheric peak altitudes In the polar hole
564 region, Radio Sci., 36, 277-285, doi:10.1029/1999rs002401, 2001.

565 Briggs, B.H., and Parkin I. A.: On the variation of radio star and satellite scintillation with zenith
566 angle, J. Atmos. Terr. Phys., 25, 339-365, doi:10.1016/0021-9169(63)90150-8, 1963.

567 Brinton, H., Grebowsky, J., and Brace L.: The high-latitude winter F-region at 300 km: Thermal
568 plasma observations from Ae-C, J. Geophys. Res., 83, 4767-4776,
569 doi:10.1029/Ja083ia10p04767, [https://doi.org/10.1016/0273-1177\(91\)90317-D](https://doi.org/10.1016/0273-1177(91)90317-D), 1978.

570 Buchau, J. and Reinisch, B. W.: Electron density structures in the polar F region, Adv. Space
571 Res., 11(10), 29-37, 1991.

572 Buchau, J., Reinisch, B. W., Weber, E. J., and Moore, J. G.: Structure and dynamics of the winter
573 polar cap F region, Radio Sci., 18, 995-1010, <https://doi.org/10.1029/RS018i006p00995>, 1983.

574 Carlson, H. C., Oksavik, K., Moen, J., van Eyken, A.P., and Guio, P.: ESR mapping of polar-cap
575 patches in the dark cusp, Geophys. Res. Lett., 29 (10), 1386, doi:10.1029/2001GL014087,
576 2002.

577 Carlson, H. C., Oksavik, K., Moen, J., and Pedersen, T.: Ionospheric patch formation: Direct
578 measurements of the origin of a polar cap patch, Geophys. Res. Lett., 31, L08806,
579 doi:10.1029/2003GL018166, 2004.

580

581 Carlson, H. C., Moen, J., Oksavik, K., Nielsen, C. P., McCrea, I. W., Pedersen, T. R., and Gallop,
582 P.: Direct observations of injection events of subauroral plasma into the polar cap, *Geophys.*
583 *Res. Lett.*, 33, L05103, doi:10.1029/2005GL025230, 2006.

584 Carlson, H., Oksavik, K., and Moen, J.: On a new process for cusp irregularity production,
585 *Ann. Geophys.*, 26, 2871-2885, doi:10.5194/angeo-26-2871-2008, 2008.

586 Cervera, M., and Thomas, R.: Latitudinal and temporal variation of equatorial ionospheric
587 irregularities determined from GPS scintillation observations, *Ann. Geophys.*, 24, 3329-3341,
588 doi:10.5194/Angeo-24-3329-2006, doi: 10.5194/angeo-24-3329-2006, 2006.

589 Chisham, G., Lester, M., Milan, S. E., Freeman, M. P., Bristow, W. A., Grocott, A., McWilliams,
590 K. A., Ruohoniemi, J. M., Yeoman, T. K., Dyson, P. L., Greenwald, R. A., Kikuchi, T., Pinnock, M.,
591 Rash, J. P. S., Sato, N., Sofko, G. J., Villain, J.-P., and Walker, A. D. M.: A decade of the Super
592 Dual Auroral Radar Network (SuperDARN): Scientific achievements, new techniques and
593 future directions, *Surv. Geophys.*, 28, 33–109, doi:10.1007/s10712-007-9017-8, 2007.

594 Cowley, S.W.H. and Lockwood, M.: Excitation and decay of solar-wind driven flows in the
595 magnetosphere-ionosphere system, *Ann. Geophys.*, 10, 103, 1992.

596 Crowley, G.: Critical Review of patches and blobs, in *Polar Cap Boundary Phenomena*, in: *URSI*
597 *Review of Radio Science 1993-1996*, edited by Stone, W. R., published for the International
598 Union of Radio Science, Oxford University Press, 619-648, doi:10.1029/2009JA014985, 1996.

599 De Franceschi, G., Spogli, L., Alfonsi, L. et al. The ionospheric irregularities climatology over
600 Svalbard from solar cycle 23. *Sci Rep* 9, 9232 (2019) doi:10.1038/s41598-019-44829-5

601 Elmas, Z., Forte, B. and Aquino, A.: The impact of ionospheric scintillation on the GNSS receiver
602 signal tracking performance and measurement accuracy, *URSI General Assembly and*
603 *Scientific Symposium*, doi 10.1109/URSIGASS.2011.6123719, 2011.

604 Forte B. (2005), Optimum detrending of raw GPS data for scintillation measurements at
605 auroral latitudes, *Journal of Atmospheric and Solar-Terrestrial Physics*, Vol. 67, N. 12,
606 doi:10.1016/j.jastp.2005.01.011.

607 Forte, B., and Radicella, S.: Problems in data treatment for ionospheric scintillation
608 measurements, *Radio Sci.*, 37, 81-85, doi:10.1029/2001rs002508, 2002.

609 Foster, J. C.: Ionospheric signatures of magnetospheric convection, *J. Geophys. Res.*, 89, 855-
610 865, 10.1029/JA089iA02p00855, 1984.

611 Fremouw, E. J., Leadabrand, R. L., Livingston, R. C., Cousins, M. D., Rino, C. L., Fair, B. C., and
612 Long, R. A.: Early results from the DNA wideband satellite experiment—Complex-signal
613 scintillation, *Radio Sci.*, 13, 167–187, doi:10.1029/RS013i001p00167, 1978.

614 Greenwald, R. A., Baker, K. B., Dudeney, J. R., Pinnock, M., Jones, T. B., Thomas, E. C., Vilain,
615 J. P., Cerisier, J. C., Senior, C., Hanuise, C., Hunsucker, R. D., Sofko, G., Koehler, J., Neilsen, E.,
616 Pellinen, R., Walker, A. D. M., Sato, N., and Yamagishi, H.: DARN/SuperDARN: A global view
617 of high latitude convection, *Space Sci. Rev.*, 71, 761-796. doi:10.1007/BF00751350, 1995.

618 Hapgood, M. (2017), Satellite navigation—Amazing technology but insidious risk: Why
619 everyone needs to understand space weather, *Space Weather*, 15, 545–548,
620 doi:10.1002/2017SW001638.

621 Jin, Y., Moen, J. I., Miloch, W. J., Clausen, L. B. N., and Oksavik, K.: Statistical study of the GNSS
622 phase scintillation associated with two types of auroral blobs, *J. Geophys. Res. Space Physics*,
623 121, doi:10.1002/2016JA022613, 2016.

624 Jin, Y., Moen, J., Oksavik, K., Spicher, A., Clausen, L., Miloch, W.: GPS scintillations associated
625 with cusp dynamics and polar cap patches. *J. Space Weather Space Clim.*, 7, A23
626 doi:10.1051/swsc/2014019, 2017.

627 Jones, D. G., Walker I. K., and Kersley, L.: Structure of the poleward wall of the trough and the
628 inclination of the geomagnetic field above the EISCAT radar, *Ann. Geophys.*, 15, 740-746,
629 <https://doi.org/10.1007/s00585-997-0740-8>, 1997.

630 Kersley, L., Russell, C. D., and Rice, D. L.: Phase scintillation and irregularities in the northern
631 polar ionosphere, *Radio Sci.*, 30, 619, doi:10.1029/94RS03175,1995.

632 Kersley, L., Jenkins, D. B., and Edwards, K. J.: *Nature Phys .Sci.*, 239, 11, 1972.

633 Keskinen, M. J. and Ossakow, S. L.: Theories of high-latitude ionospheric irregularities: A
634 review, *Radio Sci.*, 18, 1077-1091, doi:10.1029/RS018i006p01077, 1983.

635 Kinrade, J., Mitchell, C. N., Smith, N. D., Ebihara, Y., Weatherwax, A. T., and Bust, G. S.: GPS
636 phase scintillation associated with optical auroral emissions: First statistical results from the
637 geographic South Pole, *J. Geophys. Res. Space Physics*, 118, 2490–2502,
638 doi:10.1002/jgra.50214, 2013.

639 Lockwood, M., and Carlson, H. C.: Production of polar cap electron density patches by
640 transient magnetopause reconnection, *Geophys. Res. Lett.*, 19, 1731 – 1734, 1992.

641 McCaffrey, A. M., & Jayachandran, P. T. (2019). Determination of the refractive contribution
642 to GPS phase “scintillation”. *Journal of Geophysical Research: Space Physics*, 124, 1454– 1469.
643 <https://doi.org/10.1029/2018JA025759>

644 McCrea, I., Aikio, A., Alfonsi, L., Belova, E., Buchert, S., Clilverd, M., Engler, N., Gustavsson, B.,
645 Heinselman, C., Kero, J., Kosch, M., Lamy, H., Leyser, T., Ogawa, Y., Oksavik, K., Pellinen-
646 Wannberg, A., Pitout, F., Rapp, M., Stanislawski, I., and Vierinen, J.: The science case for the
647 EISCAT_3D radar, *Progress in Earth and Planetary Science*, 2:21, doi:10.1186/s40645-015-
648 0051-8, 2015.

649 Millward, G. H., Moffett, R. J., Balmforth, H. F., and Rodger, A. S.: Modeling the ionospheric
650 effects of ion and electron precipitation in the cusp, *J. Geophys. Res.*, 104, 24,603,
651 <https://doi.org/10.1029/1999JA900249>, 1999.

652 Mitchell, C. N., Alfonsi, L., De Franceschi, G., Lester, M., Romano, V., and Wernik, A. W.: GPS
653 TEC and scintillation measurements from the polar ionosphere during the October 2003
654 storm, *Geophys. Res. Lett.*, 32, L12S03, doi:10.1029/2004GL021644, 2005.

655 Nishimura, Y., Lyons, L. R., Zou, Y., Oksavik, K., Moen, J. I., Clausen, L. B., Donovan, E. F.,
656 Angelopoulos, V., Shiokawa, K., Ruohoniemi, J. M., Nishitani, N., McWilliams, K. A., and Lester,
657 M.: Day-night coupling by a localized flow channel visualized by polar cap patch propagation,
658 *Geophys. Res. Lett.*, 41, 3701-3709, doi:10.1002/2014GL060301, 2014.

659 Nishitani, N., Ruohoniemi, J. M., Lester, M., Baker, J. B. H., Koustov, A. V., Shepherd, S. G.,
660 Chisham, G., Hori, T., Thomas, E. G., Makarevich, R. A., Marchaudon, A., Ponomarenko, P.,
661 Wild, J. A., Milan, S. E., Bristow, W. A., Devlin, J., Miller, E., Greenwald, R. A., Ogawa, T.,
662 and Kikuchi, T.: Review of the accomplishments of mid-latitude Super Dual Auroral Radar
663 Network (SuperDARN) HF radars, *Prog. Earth Planet. Sci.*, 6, 27, doi:10.1186/s40645-019-
664 0270-5, 2019.

665 Obara, T., And Oya, h.: Observations of polar cusp and polar cap ionospheric irregularities and
666 formation of ionospheric holes using topside sounder onboard Exos-C (Ohzora) satellite,
667 *Journal of Geomagnetism and Geoelectricity*, 41, 1025-1042, doi:10.5636/Jgg.41.1025, 1989.

668 Oksavik, K., Barth, V. L., Moen, J., and Lester, M.: On the entry and transit of high-density
669 plasma across the polar cap, *J. Geophys. Res.*, 115, A12308, doi:10.1029/2010JA015817,
670 2010.

671 Oksavik, K., van der Meeren, C., Lorentzen, D. A., Baddeley, L. J., and Moen, J.: Scintillation
672 and loss of lock from poleward moving auroral forms in the cusp ionosphere, *J. Geophys. Res.*
673 *Space Physics*, 120, doi:10.1002/2015JA021528, 2015.

674 Parkinson, M. L., Dyson, P. L., Pinnock, M., Devlin, J. C., Hairston, M. R., Yizengaw, E., and
675 Wilkinson, P. J.: Signatures of the midnight open-closed magnetic field line boundary during
676 balanced dayside and nightside reconnection, *Ann. Geophys.*, 20, 1617-1630,
677 <https://doi.org/10.5194/angeo-20-1617-2002>, 2002.

678 Prikryl, P., Jayachandran, P. T., Chadwick, R., and Kelly, T. D.: Climatology of GPS phase
679 scintillation at northern high latitudes for the period from 2008 to 2013, *Ann. Geophys.*, 33,
680 531-545, <https://doi.org/10.5194/angeo-33-531-2015>, 2015.

681 Pryse, S. E., Wood, A.G., Middleton, H. R., McCrea, I. W., and Lester, M.: Reconfiguration of
682 polar cap plasma in the magnetic midnight sector, *Ann. Geophys.*, 24, 2201-2208,
683 <https://doi.org/10.5194/angeo-24-2201-2006>, 2006.

684 Pryse S. E., Kersley, L., and Russell C. D.: Scintillation near the F layer trough over northern
685 Europe, *Radio Science* 26, 4, 1105-1114, <https://doi.org/10.1029/91RS00490>, 1991.

686 Rideout, W. and Coster, A. J.: Automated GPS processing for global total electron content
687 data, *GPS Solutions*, 10, 219-228, <https://doi.org/10.1007/s10291-006-0029-5>, 2006.

688 Rino, C. L., Livingston, R. C., Tsunoda, R. T., Robinson, R. M., Vickrey, J. F., Senior, C., Cousins,
689 M. D., Owen, J., and Klobuchar, J. A.: Recent studies of the structure and morphology of
690 auroral-zone F-region irregularities, *Radio Sci.*, 18, 1167-1180, 10.1029/RS018i006p01167,
691 1983.

692 Rodger, A. S., Pinnock, M., Dudeney, J. R., Baker, K. B., and Greenwald, R. A.: A new
693 mechanism for polar patch formation, *J. Geophys. Res.*, 99, 6425-6436,
694 doi:10.1029/93JA01501, 1994.

695 Ruohoniemi, J. M., and Greenwald, R. A.: Dependencies of high- latitude plasma convection:
696 Consideration of interplanetary magnetic field, seasonal, and universal time factors in
697 statistical patterns, *J. Geophys. Res.*, 110, A09204, doi:10.1029/2004JA010815, 2005.

698 Smith, A. M., Mitchell, C. N., Watson, R. J., Meggs, R. W., Kintner, P. M., Kauristie, K., and
699 Honary, F.: GPS scintillation in the high arctic associated with an auroral arc, *Space Weather*,
700 6, S03D01, doi:10.1029/2007SW000349, 2008.

701 Sojka, J., Bowline, M., Schunk, R., Decker, D., Valladares, C., Sheehan, R., Anderson, D., and
702 Heelis, R.: Modeling Polar Cap F-Region Patches Using Time Varying Convection, *Geophys.*
703 *Res. Lett.*, 20, 1783-1786, Doi:10.1029/93gl01347, 1993.

704 Spogli, L., Alfonsi, L., De Franceschi, G., Romano, V., Aquino, M. H. O., and Dodson, A.:
705 Climatology of GPS ionospheric scintillations over high and mid-latitude European regions,
706 *Ann. Geophys.*, 27, 3429-3437, <https://doi.org/10.5194/angeo-27-3429-2009>, 2009.

707 Thomas, E. G., and Shepherd, S. G.: Statistical patterns of ionospheric convection derived from
708 mid-latitude, high-latitude, and polar SuperDARN HF radar observations, *J. Geophys. Res.*,
709 123, 3196–3216, <https://doi.org/10.1002/2018JA025280>, 2018.

710 Tsunoda, R. T.: High-latitude F region irregularities: A review and synthesis, *Rev. Geophys.*,
711 26, 719-760, <https://doi.org/10.1029/RG026i004p00719>, 1988.

712 Valladares, C. E., Decker, D. T., Sheehan, R., Anderson, D. N., Bullett, T. and Reinisch, B. W.:
713 Formation of polar cap patches associated with north-to-south transitions of the
714 interplanetary magnetic field, *J. Geophys. Res.*, 103, 14657-14670,
715 <https://doi.org/10.1029/97JA03682>, 1998.

716 Valladares, C.E., Basu, S., Buchau, J., and Friis-Christensen, E.: Experimental evidence for the
717 formation and entry of patches into the polar cap, *Radio Sci.*, 29, 167-194, doi:
718 10.1029/93RS01579, 1994.

719 van der Meeren, C., Oksavik, K., Lorentzen, D., Moen, J. I., and Romano, V.: GPS scintillation
720 and irregularities at the front of an ionization tongue in the night-side polar ionosphere, *J.*
721 *Geophys. Res. Space Physics*, 119, 8624–8636, doi:10.1002/2014JA020114, 2014.

722 van der Meeren, C., Oksavik, K., Lorentzen, D. A., Rietveld, M. T., and Clausen, L. B. N.: Severe
723 and localized GNSS scintillation at the poleward edge of the nightside auroral oval during
724 intense substorm aurora, *J. Geophys. Res. Space Physics*, 120, 10,607–10,621,
725 doi:10.1002/2015JA021819, 2015.

726 van der Meeren, C., Oksavik, K., Lorentzen, D. A., Paxton, L. J., and Clausen, L. B. N.: Scintillation
727 and irregularities from the nightside part of a Sun-aligned polar cap arc, *J. Geophys. Res. Space*
728 *Physics*, 121, 5723–5736, doi:10.1002/2016JA022708, 2016.

729 Vierinen, J., Coster, A. J., Rideout, W. C., Erickson, P. J., and Norberg, J.: Statistical framework
730 for estimating GNSS bias, *Atmos. Meas. Tech. Discuss.*, 8, 9373–9398, doi:10.5194/amtd-8-
731 9373-2015, 2015.

732 Wang, Y., Zhang, Q. - H., Jayachandran, P. T., Moen, J., Xing, Z. - Y., Chadwick, R., et al. (2018).
733 Experimental evidence on the dependence of the standard GPS phase scintillation index on
734 the ionospheric plasma drift around noon sector of the polar ionosphere. *Journal of*
735 *Geophysical Research: Space Physics*, 123, 2370–2378.
736 <https://doi.org/10.1002/2017JA024805>

737 Wannberg, G., Wolf, I., Vanhainen, L.-G., Koskenniemi, K., Röttger, J., Postila, M., Markkanen,
738 J. Jacobsen, R., Stenberg, A., Larsen, R., Eliassen, S., Heck, S., and Huuskonen, A.: The EISCAT

739 Svalbard radar: A case study in modern incoherent scatter radar system design, *Radio Sci.*, 32,
740 2283–2308, doi:10.1029/97RS01803, 1997.

741 Walker, I. K., Moen, J., Kersley, L., and Lorentzen, D. A.: On the possible role of cusp/cleft
742 precipitation in the formation of polar-cap patches, *Ann. Geophys.*, 17, 1298-1305,
743 doi.org/10.1007/s00585-999-1298-4, 1999.

744 Weber, E., Buchau, J., Moore, J., Sharber, J., Livingston, R., Winningham, J., and Reinisch, B.:
745 F-layer ionization patches in the polar cap, *J. Geophys. Res.*, 89, 1683,
746 doi:10.1029/Ja089ia03p01683, 1984

747 Zwickl, R. D., Doggett, K.A., Sahm, S., Barrett, W.P., Grubb, R.N., Detman, T.R., Raben, V.J.,
748 Smith, C.W., Riley, P., Gold, R.E., Mewaldt, R.A., Maruyama T.: The NOAA Real-Time Solar-
749 Wind (RTSW) system using ACE data, *Space Sci. Rev.*, 86, 633–648, doi:10.1023/
750 A:1005044300738, 1998.